Journal of Power Sources 189 (2009) 1083–1092

Contents lists available at ScienceDirect

Journal of Power Sources

journal homepage: www.elsevier.com/locate/jpowsour

Development of bipolar plates with different flow channel configurations for fuel cells

Rajesh Boddu, Uday Kumar Marupakula, Benjamin Summers, Pradip Majumdar*

Department of Mechanical Engineering, Northern Illinois University, DeKalb, IL 60115, USA

ARTICLE INFO

Article history:
Received 4 December 2008
Received in revised form 27 December 2008
Accepted 30 December 2008
Available online 22 January 2009

Keywords:
Bipolar plates
Fuel cell

ABSTRACT

Bipolar plates include separate gas flow channels for anode and cathode electrodes of a fuel cell. These gases flow channels supply reactant gasses as well as remove products from the cathode side of the fuel cell. Fluid flow, heat and mass transport processes in these channels have significant effect on fuel cell performance, particularly to the mass transport losses. The design of the bipolar plates should minimize plate thickness for low volume and mass. Additionally, contact faces should provide a high degree of surface uniformity for low thermal and electrical contact resistances. Finally, the flow fields should provide for efficient heat and mass transport processes with reduced pressure drops. In this study, bipolar plates with different serpentine flow channel configurations are analyzed using computational fluid dynamics modeling. Flow characteristics including variation of pressure in the flow channel across the bipolar plate are presented. Pressure drop characteristics for different flow channel designs are compared. Results show that with increased number of parallel channels and smaller sizes, a more effective contact surface area along with decreased pressured drop can be achieved. Correlations of such entrance region coefficients will be useful for the PEM fuel cell simulation model to evaluate the affects of the bipolar plate design on mass transfer loss and hence on the total current and power density of the fuel cell.

1. Introduction

Fuel cells have received considerable attention in recent times as one of the most attractive alternative power generation systems in a wide variety of applications to decrease our dependency on fossil fuels. However, major obstacles to the adaptation of this technology are the excessive cost, lackluster performance at high current densities, and durability over an extended period of time. Some of the major challenges are to improve the over fuel cell efficiency, improve performance, and increase reliability and durability of some of the key components such as the Membrane Electrode Assembly (MEA) and the bipolar plate.

A fuel cell is an electrochemical device that uses electrochemical reaction with hydrogen and oxygen, and produces electricity directly. Only by-products of this reaction are water and heat. Bipolar plates include separated flow channels to supply hydrogen and oxygen reactant gasses to anode and cathode electrodes, respectively. It also connects the cathode of a tri-layer fuel cell to the anode of the next tri-layer fuel cell in order to provide an efficient collection and transmission of current through the cells. Fig. 1 shows a typical tri-layer MEA along with bipolar plates. The gas flow field design also play a critical role in the effective removal of water and heat generated during the electrochemical reactions, and to some extent for the removal of any corroded ions from the metallic bipolar plates or any metallic interconnect materials. Fig. 1 shows a typical tri-layer MEA along with bipolar plates.

The bipolar plate should be thin with uniform contact surfaces at the electrodes for reduced electrical and thermal resistances. Additionally, it should provide for efficient mass transport of reactant gasses to gas diffusion layers of the electrodes with reduced pressure drop, thus resulting in uniform current distributions, high total current and high power density.

The gas flow field design in a bipolar plate has a significant effect on the variation of pressure of the gases along the channel and on the mass transport rates of reactant gases and products to and from the electrode surfaces, and significantly affects the fuel cell mass transfer loss and the output voltage. The mass transfer loss results in a decrease in fuel cell output voltage when gas flow field and conditions cannot sustain a high mass transport rate to supply the reactants and remove the products to and from the electrode reaction sites, respectively. This is more critical for the operation of the fuel cell at higher current density, which is desirable for achieving higher power density. An effective design of gas flow field, through optimization of the channel dimensions, shape and configuration may results in an improved bipolar plate.

* Corresponding author.
E-mail address: majumdar@ceet.niu.edu (P. Majumdar).

0378-7753/$ – see front matter © 2009 Elsevier B.V. All rights reserved.
doi:10.1016/j.jpowsour.2008.12.156

Nomenclature

a_a	width of anode
a_c	width of cathode
a_{ae}	width of electrolyte
C_p	pressure coefficient
w	width of the channel
h	height of the channel
H	height of the bipolar plate
P_{in}	inlet pressure
P_{out}	outlet pressure
Re	Reynolds number
Nx	number of nodes in x-direction
Ny	number of nodes in y-direction
Nz	number of nodes in z-direction
V	average velocity in the channel
u_{in}	inlet velocity
P_{in}	inlet pressure
D_h	hydraulic diameter

Greek symbols

μ	viscosity
ρ	density of the gas

The effective contact surface area of the reactant gas or the land area of the electrode surface, has a direct affect on the gas concentration distributions in the electrodes, and hence on overall electrochemical reaction. The fluid flow, heat and mass transfer phenomena play a key role in the design of the high performance bipolar plate gas flow field.

Kumar and Reddy [1] used a three-dimensional half-cell computational model to study the effect of size and shape of a single serpentine channel on the hydrogen consumption rate at the anode electrode. Improved performance of a polymer electrolyte membrane fuel cell (PEMFC) was achieved through optimization of the channel dimensions and shape of the flow field. Results showed increase in hydrogen consumption rate with decrease in land width. Kumar and Reddy [2] considered metallic bipolar plates with conventional flow channels, embedded with metal-foams in the flow fields. Results show superior performance of the fuel cell with the use of embedded metal foam bipolar plates that results in a lower permeability.

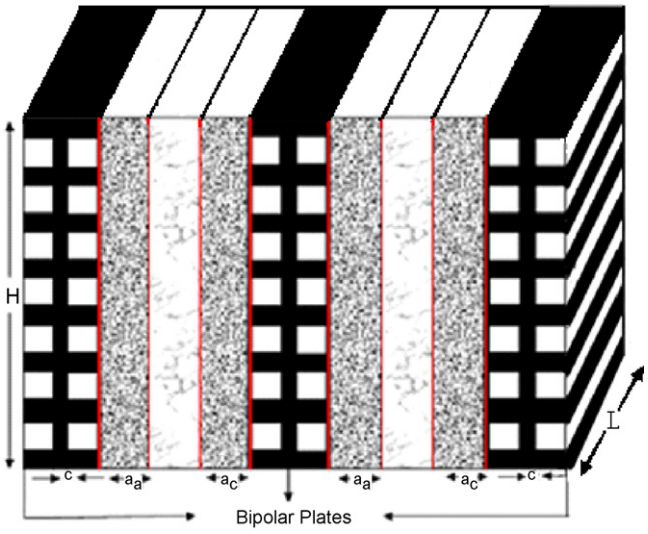

Fig. 1. Tri-layer fuel cell with the series of bipolar plates.

Kumar and Reddy [3] used SS-316 bipolar plates with multiple parallel straight channels in their fabrication of a two-cell PEM fuel cell stack. A stable operation for over 1000 h of continues operation and an effective removal of corroded Fe ions by the gas flow field were demonstrated with this multi-parallel channel design.

Wheeler et al. [4] utilized a porous bipolar plate design to transfer liquid water from cell to coolant stream as a passive means for water management in a PEM fuel cell. Curtis and Xianguo [5] used transport correlations in the computational model for the reactant gas transport in flow channels of graphite bipolar plates and demonstrated mass transfer limitation as the major cause of cell performance loss.

Djilali and co-workers [6] developed a three-dimensional PEM fuel cell model by incorporating a parallel straight gas channels. In order to reduce the computation cost, the model was based on geometric periodicity of fuel cell and by considering a computational domain that starts from mid-plane of one flow channel to mid-plane of the adjacent land area. Nguyen et al. [7] used a three-dimensional computational fluid dynamics model of a PEM fuel cell with serpentine flow field channels and demonstrated the effect of the gas flow channel design on the variation of gas concentration and local current distribution patterns at different loads. The computational domain was also limited to a single turn of the serpentine channel. As we can see that most of the computational fuel cell model presented in recent literatures assumed similar approach in incorporating gas flow channels. However, a more accurate computation of gas concentration distributions and local current distributions on electrode surface require evaluation of entrance region transport phenomena. This is necessary in order to take account of local variation of reactant gas concentration and current density over electrode surfaces.

The primary objective of our research is to develop bipolar plate that not only provides high contact surface area for maintaining a more uniform gas concentration distribution, but also provides high performance gas flow field to achieve enhanced heat and mass transport rates without increasing the pressure drop significantly, and hence reduce the mass transfer loss for operation of the PEM fuel cell at high current density. A number of bipolar plate designs of varying geometry and configurations will be evaluated using a computational model based on three-dimensional developing flow, heat and mass transport. This model has been used by Boddu and Majumdar [8] for evaluating bipolar plate design with straight through channels. In this paper, results for the bipolar plate with different serpentine flow channel design are presented. A sensitivity study is conducted with different bipolar plate designs, and varying geometrical parameters. Flow characteristics including variation of pressure in the flow channel across the bipolar plate are presented. Pressure drop characteristics for different flow channel designs are compared. Correlations of such entrance region coefficients will be useful for the PEM fuel cell simulation model to evaluate the affects of the bipolar plate design on mass transfer loss and hence on the total current and power density of the fuel cell.

2. Mathematical model

Fluid flow and heat transfer analysis of a bipolar plate design with different serpentine flow channels are considered in this study. The three-dimensional flow configuration and geometry of the serpentine channels are depicted in Fig. 2. The fluid enters through the header inlet and then enters different interior gas channels and flows out from the header outlet. The current densities as well as the activation losses depend on the primary contact surface area of the gas channels adjacent to the gas diffusion layer.

The rest of the contact area is referred to as the land area. As gas enters the gas diffusion layer, it diffuses towards the reaction surfaces as well as into the land area to some extent. The overall per-

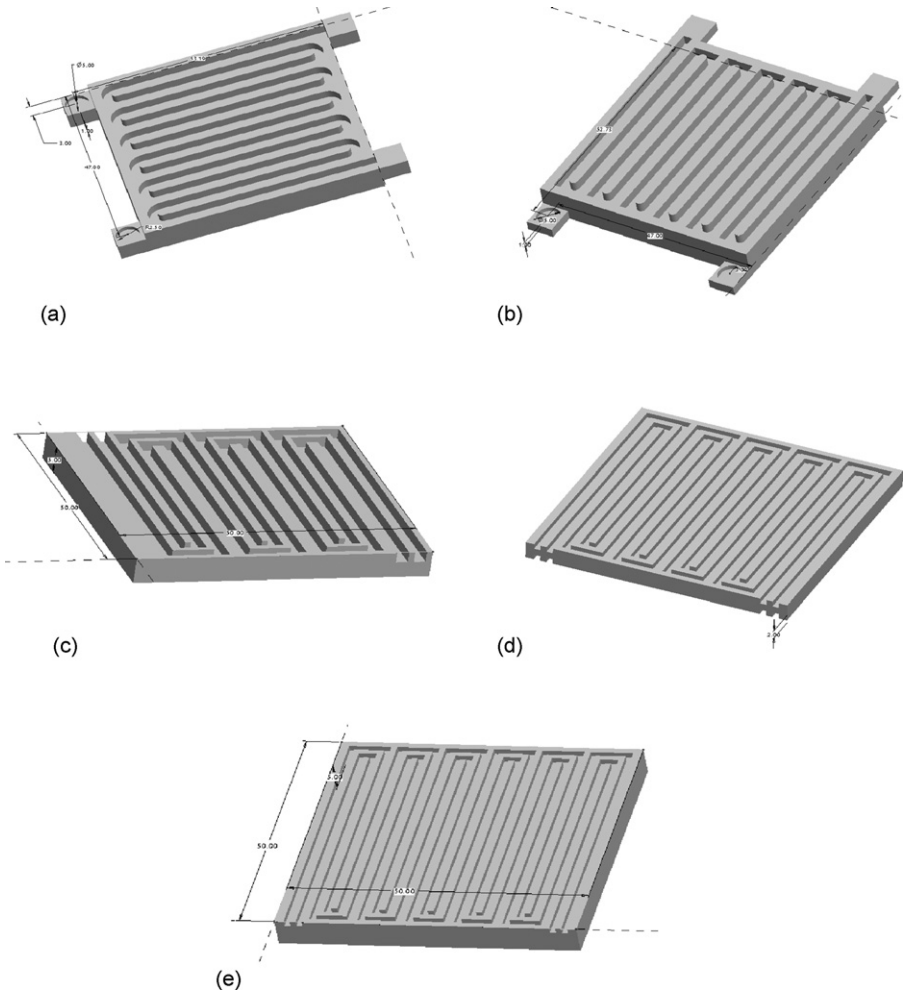

Fig. 2. Serpentine flow channels (a) single channel curvilinear bends, (b) single channel square bends, (c) dual serpentine channels with width 2 mm, (d) dual serpentine channels with width 1.2 mm and (e) dual serpentine channels with 1 mm size.

formance of the fuel cell is directly proportional to the area of the gases in contact with the bipolar plate. Five different configurations are considered as demonstrated in Fig. 2, and this includes: single serpentine channel with curvilinear bends, single serpentine channel with square bends, multiple serpentine channels with square bends. For dual serpentine channel with square bends, two sizes 1.2 and 1 mm are considered.

2.1. Single serpentine channels

In serpentine channels the effective consumption of gases for the reaction is increased as compared to the straight through channels. The overall contact surface area on bipolar plate varies as the channel configuration, numbers and size are changed. For the channel size of 2 mm, it consists of 11 bends with 12 gas channels and 13 solid channels of varying lengths. For serpentine channels, the effective contact surface area of the gas channels can be increased by replacing circular bends with square bends as shown in Fig. 2b.

2.2. Dual serpentine channels with square bends

Since the serpentine channel with square bends provides more effective contact area, multiple parallel serpentine channels are considered with square bends. For similar dimensions from the above model, the channels cover approximately 75% area of the bipolar plate. A schematic view of the channels with width 2 mm is shown in Fig. 2c. Since the channels cover approximately 80% the overall area of the bipolar plate, the dimension of the channels is reduced in such a manner that the channels fit into the bipolar plate effectively. Upon using the trial and error method, channels with width 1.2 mm fit the bipolar plate exactly, covering the whole area on the bipolar plate as shown in Fig. 2d. For dual serpentine channels with 1.2 mm width, the number of gas channels and solid channels are 20 with varying length. There are 9 long square bends and 9 short square bends, as shown in Fig. 2d. The effective reactant area on the bipolar plate is increased by 0.56% upon increasing the channels to 20 of varying lengths. Some more improvements have been made to the previous design by reducing the channel width to 1 mm using the trial and error method. For dual serpentine channels with 1 mm width, the number of gas channels and solid channels are 24 with varying length. There are 11 long square bends and 11 short square bends, as shown in Fig. 2e.

2.3. Governing equations

Working fluid for this study is assumed to be air with a range of flow rates given in Table 1. With this range of flow rates and channel sizes, the Reynolds number of the flow varies from 3000 to 20,000, and this necessitates the need for considering the flow as turbulent. A turbulent flow is desirable for the point of enhanced mixing and enhanced heat and mass transport coefficients in the gas flow channels. In this study, the flow is assumed to be steady,

Table 1
Range of gas flow rates and inlet pressure conditions.

Case	Mass flow rate (kg s^{-1})	Inlet static pressure (psi)
I	0.0003	30
II	0.0004	30
III	0.0005	30
IV	0.00065	30
V	0.0007	30

incompressible, turbulent, and developing. The Navier-Stokes (NS) equations with constant viscosity are used to analyze gas flow in channels for the bipolar plate models. The standard $\kappa - \varepsilon$ model is used for the turbulent kinetic energy (κ) and dissipation rate (ε). The energy and mass transfer equations are based thermally entry length.

2.4. Inlet and boundary conditions

- Inlet conditions: $u = u_{in}$, $P = P_{in}$;
- Boundary conditions: No slip conditions for velocity at all walls.
- Dimensionless parameters:
  - Reynolds number: Reynolds number (Re) is defined as

$$\mathrm{Re} = \frac{\rho V D_h}{k} \tag{1}$$

  - Pressure coefficient: Pressure coefficient (C_p) is the ratio between the pressure-difference at certain location to the fluid kinetic energy:

$$C_p = \frac{p - p_\infty}{1/2\rho V^2} \tag{2}$$

3. Computational model

The mathematical model for studying the hydro-dynamically developing flow field and developing heat and mass transport phenomena is solved using FLUENT commercial code for different bipolar plate designs. GAMBIT is used as a graphical user interface (GUI) for building the model, meshing and assigning zone types to the model. A three-dimensional model is created along the x-axis with the flow field along z-direction. The geometric modeling of the problem is shown in Fig. 3.

3.1. Physical representation of the problem

A three-dimensional flow is considered for all the design options which have been mentioned in the study. Computational domain is depicted in Fig. 3. At the inlet, pressure boundary condition is given with the mass flow rate specified at outlet. For heat and mass transfer the top wall is maintained at higher temperature than the inlet fluid temperature. The rest of the walls are maintained at adiabatic condition, where the net heat flux is zero.

Edge meshing is performed, considering the distance from the wall. Mapped meshing is done for the straight sections along with the tet/hybrid meshing at the circular cross-section. A soft non-uniform grading scheme is used for edge meshing. The meshing is uniform throughout the model except it is more refined near the walls. An 8-node hexagonal brick type of control volume is used for rectangular channels.

A 10-node pentagonal prism and 10-node clipped cube are used for circular faces in the control volume. The computational meshes for the bipolar plate models are presented in Fig. 4.

Static pressure and scalar properties of the flow are defined at the pressure inlet boundaries. At the outlet mass flow rate is specified. The mass flow outlet adjusts the exit pressure such that a target mass flow rate (i.e. mass flow at the inlet) is obtained at convergence. The top wall of the channel is maintained at a constant surface temperature and the rest of the walls are subjected to adiabatic condition.

An implicit segregated solver is used for the study, as it requires less computational time as compared to other solving techniques.

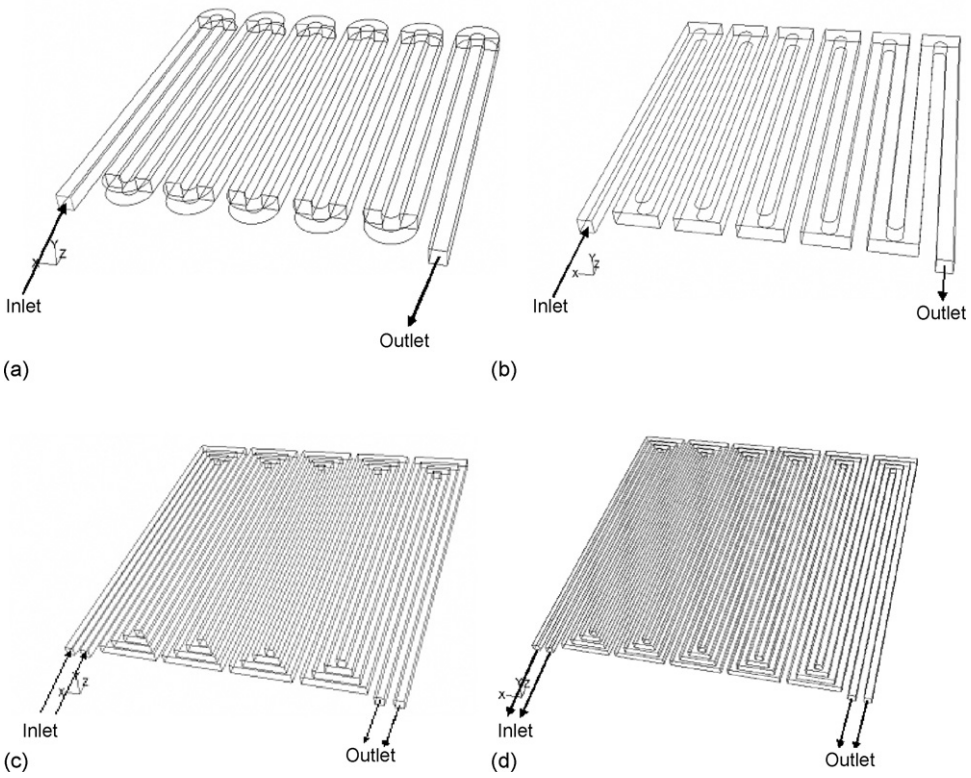

Fig. 3. Computational domain in GAMBIT model for all the chosen models for the bipolar plate.

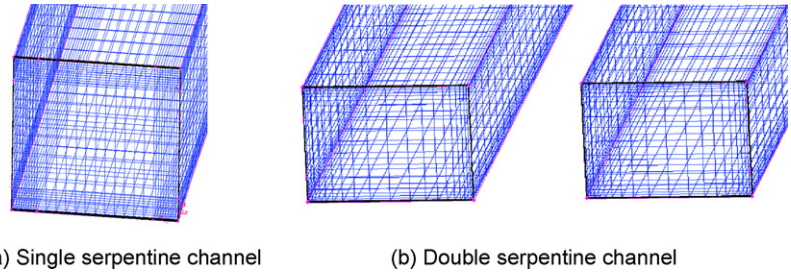

Fig. 4. Computational mesh used for serpentine channel analysis: (a) single serpentine channel and (b) double serpentine channel.

A sequential solution of the governing equations for mass and momentum and energy is obtained using the SIMPLE algorithm. The solution is iterated until the specified convergence criterion of 10^{-6} is reached. For the present study, the implicit form of linearization is considered because the explicit option is not supported by segregated solver. In this method each discrete governing equation is linearized implicitly with respect to the equation's dependent variable. This resulting system of linear equations is solved using the Successive over relaxation (SOR) method in conjunction with an algebraic multi-grid (AMG) method. Following under relaxation factors are used: pressure (0.3), momentum (0.6), turbulence kinetic energy (0.8), turbulence dissipation rate (0.8) and energy (0.9).

A second-order upwind discretization scheme for convective terms and a three-point second-order-central difference scheme for diffusion terms are used in discretization of the governing equations. The standard pressure interpolation scheme that computes face pressure as the average of pressure values in adjacent cells is used.

4. Results and discussions

Fluid flow and heat and mass transfer characteristics in the bipolar plate flow channels are analyzed in this section. The range of mass flow rates considered in this study was based on a current density range of 1.0–2.0 A cm^{-2} and a stoichiometric ratio of 1.5–3.0. Such an operating conditions lead to a very high velocity in the inlet and out feeder sections.

The distributions of pressure, velocity and temperature are studied and correlations are obtained for a range of operating parameters. The results include mesh refinement study, analysis of flow and heat transfer phenomenon in the channels of the bipolar plate.

4.1. Mesh refinement study

4.1.1. Serpentine channel

The serpentine channels are meshed using hexagonal elements with non-uniform mesh size distribution, as shown in Fig. 4a. More refined meshes are used near the solid wall where higher gradients of velocity and pressure exist. Mesh size distribution considered for these refinement study are $18 \times 18 \times 100$, $22 \times 22 \times 75$, $22 \times 22 \times 100$, $22 \times 22 \times 150$, and $25 \times 25 \times 100$. The variation of pressure coefficient is studied along the length and bends of the channel with different mesh size distribution and results are presented in Fig. 5. Results show improved convergence for the mesh distribution of $25 \times 25 \times 100$ with the associated percent relative error less than 0.02% at all locations. With further refinements, the percent relation error shows continuous increase. The rest of the computations are carried out with this mesh size distribution.

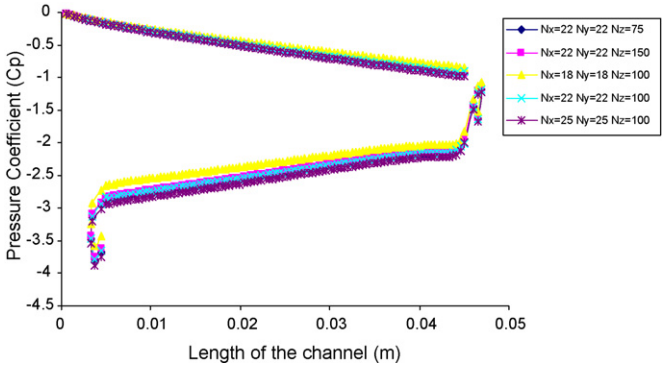

Fig. 5. Comparison of pressure coefficient curves for different meshes.

4.1.2. Dual serpentine channels

The dual serpentine channels are meshed with the hexagonal elements with non-uniform mesh size distribution, as shown in Fig. 4b. Mesh size distributions considered for both channels

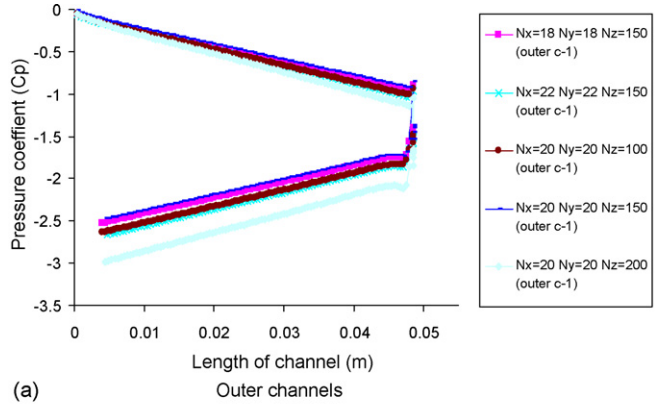

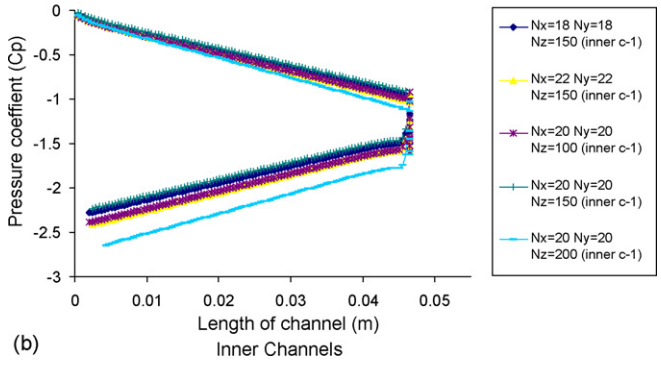

Fig. 6. Comparison of pressure coefficient curves for different meshes for dual channels: (a) outer channels and (b)inner channels.

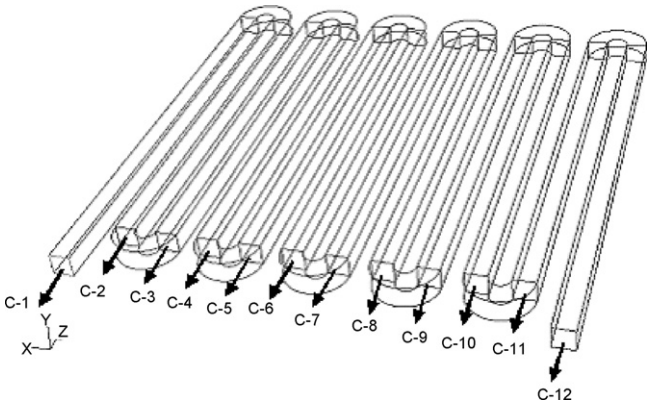

Fig. 7. Single serpentine channel design.

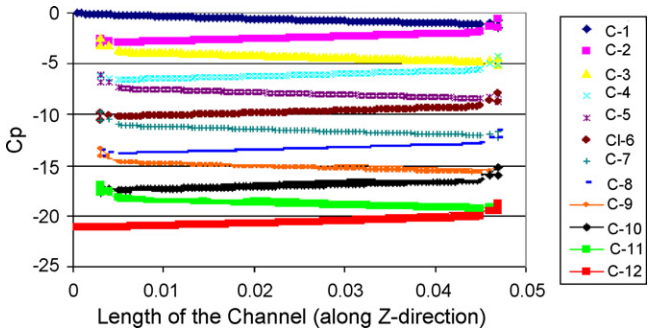

Fig. 9. Variation of coefficient of pressure along the channel.

are $18 \times 18 \times 150$, $20 \times 20 \times 100$, $22 \times 22 \times 150$, and $20 \times 20 \times 200$. Variation pressure coefficient is studied with different mesh size distribution and results are presented in Fig. 6a and b. Results show improved convergence for the mesh distribution of $22 \times 22 \times 150$ and the associated percent relative error is less than 0.02% at all locations. The rest of the computations are carried out with this mesh size distribution.

4.2. Analysis of flow field for serpentine channels

A schematic view of the bipolar plate with single serpentine channel design is shown in Fig. 7. The channels are numbered for presentation and discussion of the results. In this section, results for serpentine channels are analyzed by pressure and velocity contours. The operating mass flow rates ranges from 0.003 to 0.0007 kg s^{-1} with inlet pressure of 30 psi.

Contour plots for pressure and velocity for mass flow rate 0.0005 kg s^{-1} at an inlet static pressure 30 psi is presented in Fig. 8. It can be noticed from the contour plots that the serpentine channels give rise to additional losses due to the presence of secondary flows near the inner side the bends. However, flow displays a periodically fully developed flow by the second and third turns.

A closer look at the pressure drop data show developing flow phenomena in each channel. However, when the total pressure drop each channel is considered, a periodic fully developed pressure drop is noticed beyond the third channel. Coefficient of pressure data presented in Fig. 9 displays periodically fully developed pressure drop characteristics. The coefficient of pressure value based on pressure drop in each periodic loop shows a fully developed value of 0.58 by the third periodic loop.

4.3. Analysis of flow field for serpentine channels with square bends

A schematic view of the single serpentine channel with square bends is shown in Fig. 10. In this section, results for serpentine chan-

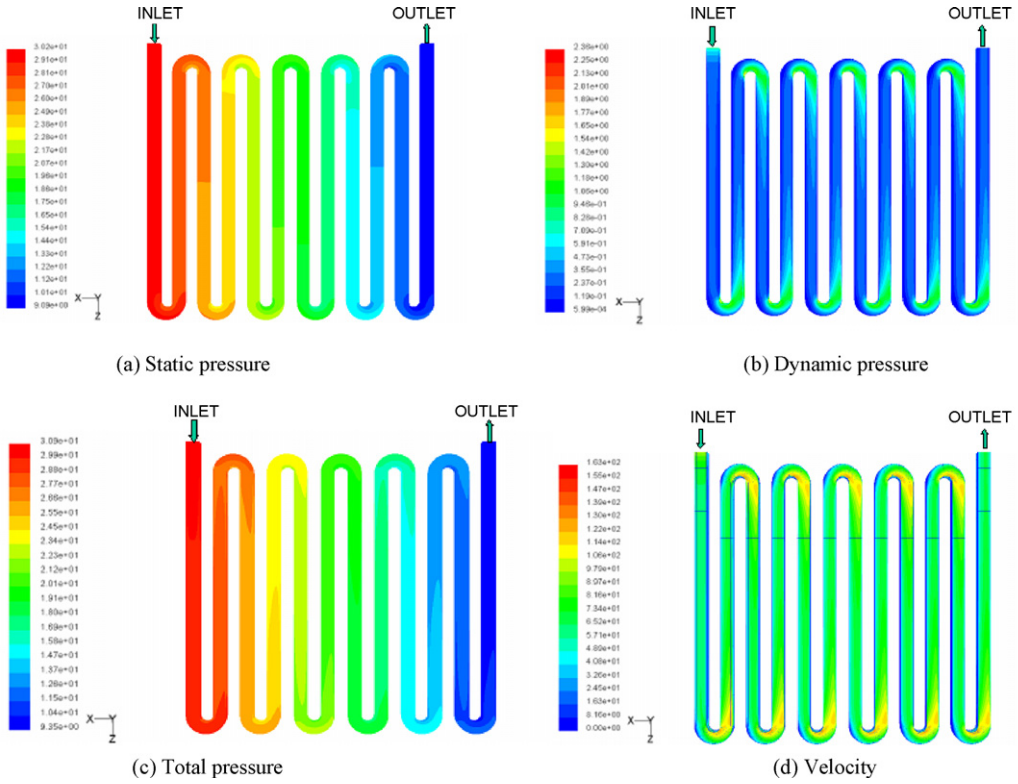

Fig. 8. Contour plots for pressure and velocity for mass flow rate 0.0005 kg s^{-1}: (a) static pressure; (b) dynamic pressure; (c) total pressure; (d) velocity magnitude.

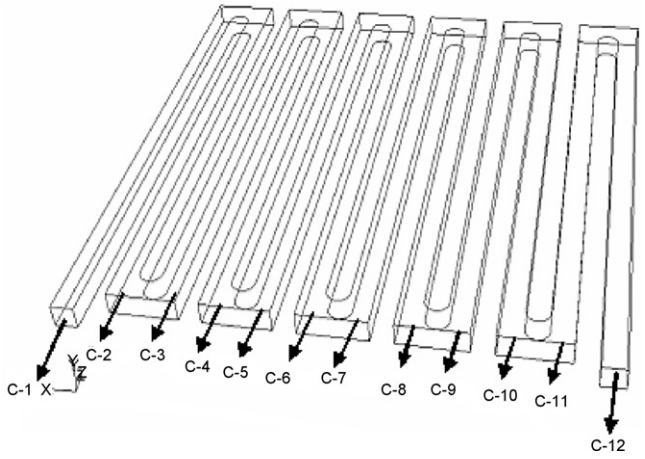

Fig. 10. Serpentine channel design with square bends: (a) static pressure; (b) dynamic pressure; (c) total pressure; (d) velocity magnitude.

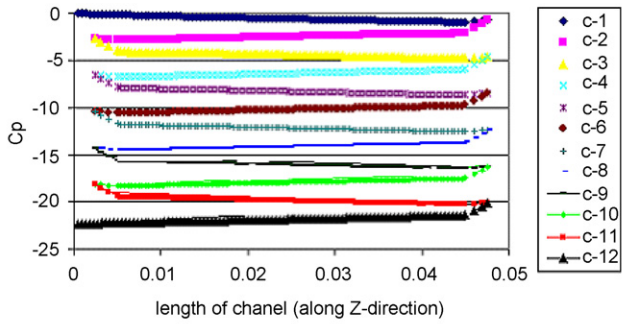

Fig. 12. Variation of pressure coefficient along the channel. *Note*: The odd numbered channels are along +ve *z*-direction. The even numbered channels are along –ve *z*-direction.

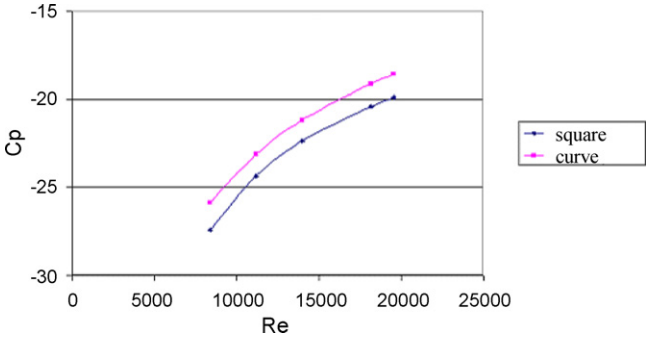

Fig. 13. Comparison of coefficient of pressure correlations for different serpentine geometry.

nels are analyzed by pressure and velocity contours, as shown in Figs. 11 and 12. The operating conditions are same as those of the serpentine channels with curvilinear bends.

Coefficient of pressure data is presented in Fig. 12. It can be noticed from the contour plots that serpentine channels with square bends also display strong secondary flows near the inner side of each bend as well as periodic fully developed flows. However, flow displays a periodically fully developed flow in the second and third turns.

Comparison of serpentine curvilinear and serpentine square bends in terms of pressure drop with increasing Reynolds number is shown in Fig. 13. The square bends exhibit consistently lower pressure drops compared to curvilinear bends. This is mainly due

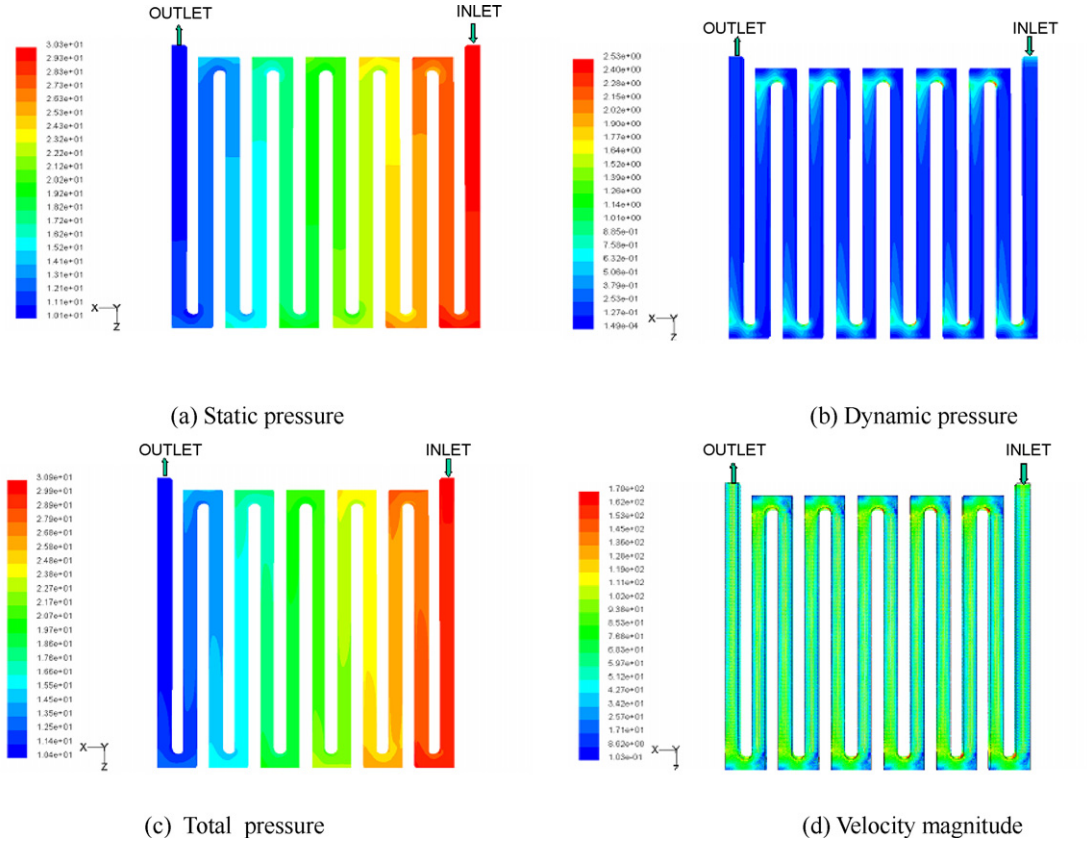

Fig. 11. Contour plots for single serpentine channel with square bends.

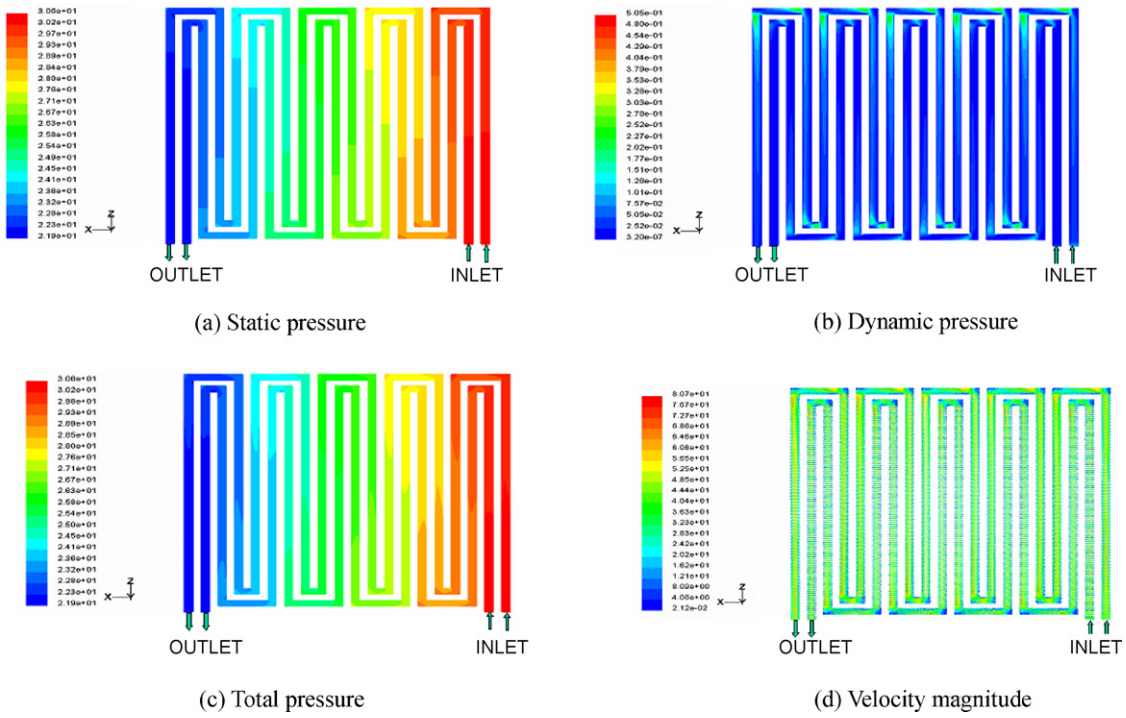

Fig. 14. Contour plots for dual channels: (a) static pressure; (b) dynamic pressure; (c) total pressure; (d) velocity magnitude.

to decreased flow lengths with sharper corners, even though there are increased flow separations around the square bends.

4.4. Analysis of flow field in multiple parallel serpentine channels with square bends

The design option-IV is a multiple parallel serpentine channel with square bends, as shown in Fig. 3d. The main idea for considering the multiple parallel serpentine channels is to increase contact surface area with the electrode surface, but with reduced pressure drops. Two different square channel sizes, 1.2 mm and 1 mm, are considered. It is expected that a decrease in cross-sectional area would lead to a more uniform distribution gas concentration at electrode surfaces. The lowest size will only be limited by the machining and fabrication processes. Contour plots for pressure and velocity are presented in Fig. 14.

It can be noticed from the contour plots that the dual serpentine channels give rise to similar periodically fully developed flow in

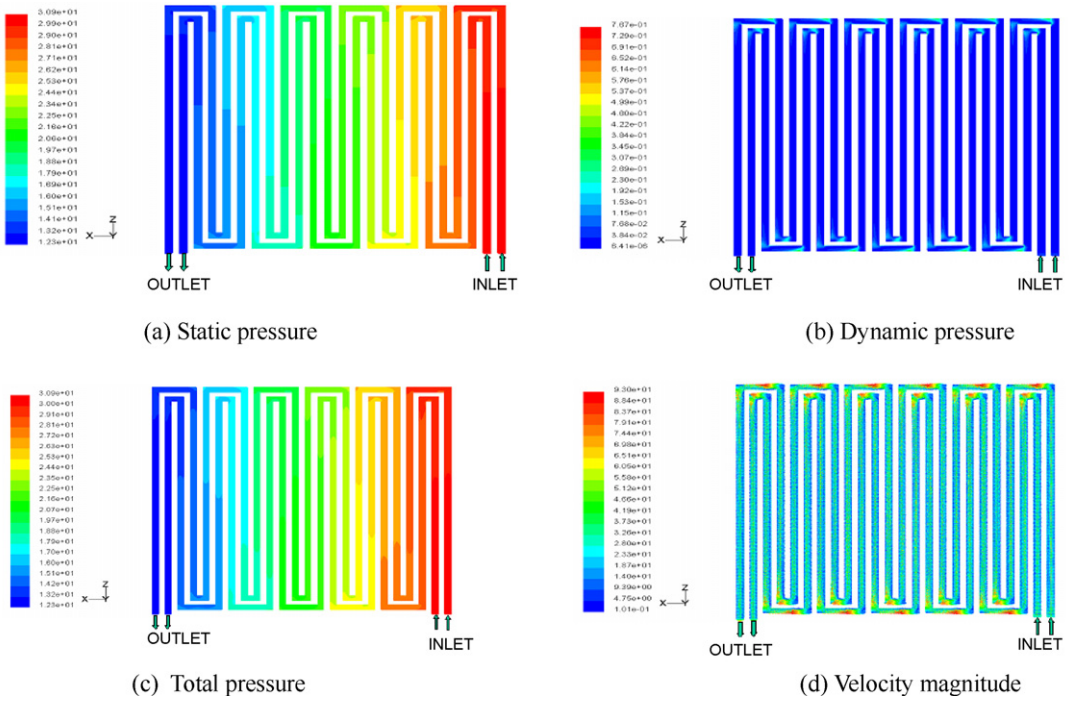

Fig. 15. Contour plots for dual serpentine channel with square bends: (a) static pressure; (b) dynamic pressure; (c) total pressure; (d) velocity magnitude.

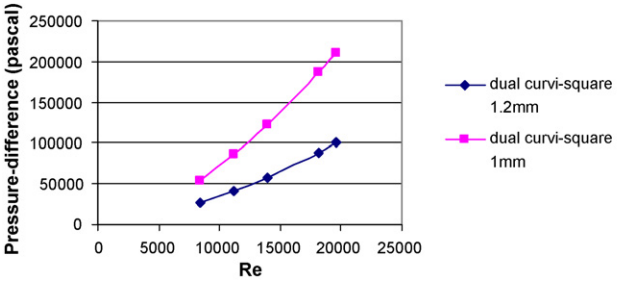

Fig. 16. Comparison of pressure drop for multiple parallel serpentine channel with different sizes.

second and third turn. However, presence of flow separations and secondary flows in each bend is significantly reduced compared to single square serpentine channels.

In order to increase the contact surface area further, the size of the dual square serpentine channel is reduced to 1 mm. Contour plots for pressure and velocity are presented in Fig. 15. Results show further reduction in flow separation and recirculation decrease in the square channels.

Pressure drop data for dual parallel serpentine channels and with two different channel sizes for a range of operating Reynolds number are presented in Fig. 16. Results show that pressure drop increases in a power law manner with increase in flow Reynolds number. As expected, pressure drop is higher for reduced channel sizes due to increased average velocity even though the flow separations are reduced in bends for smaller sizes. For example, the increases in pressure drop at a Re = 7500 is about 4.4%. The percent increase is even higher at a higher Reynolds number. For example, the increases in pressure drop at a Re = 8382 is about 33.33%.

4.5. Pressure drop comparison for different bipolar plate designs

In this section a comparison of all bipolar plate designs is provided in terms of the total pressure drop across the plates and percent of contact surface area and volume of the plate. Fig. 17 shows the pressure drop over a range of operating Reynolds number for different bipolar plates. Results show that highest pressure drop is in single curvilinear serpentine channels. Pressure drop is reduced, if we consider a single curvi-square serpentine channel of same size.

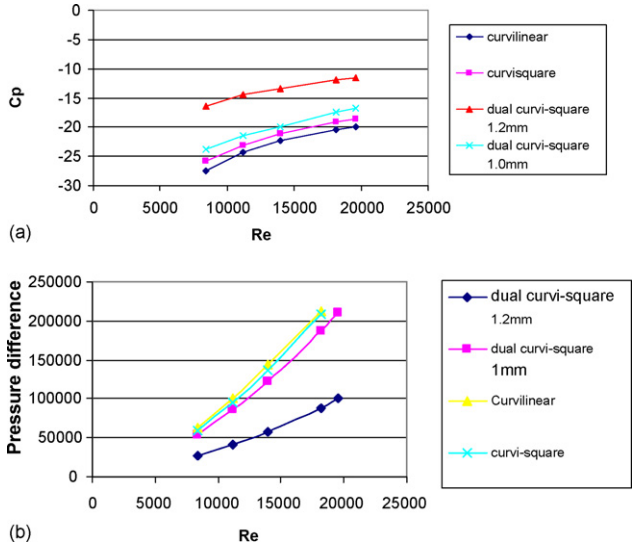

Fig. 17. Comparison of pressure drop in different bipolar plate designs.

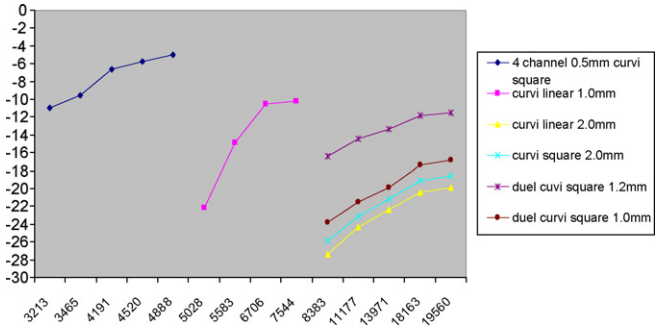

Fig. 18. Comparison of pressure drop in different bipolar plate designs including dual and four channels configurations.

The pressure drop is reduced significantly as we consider a dual curvi-square serpentine channel. The percent reduction is about 67%. When the dual curvi-square serpentine channel is optimized to increase contact surface area, the area is increased by 0.24 and the pressure drop is increased by 31.22%. However, the pressure drop is still less than that of the single curvilinear and curvi-square serpentine channels.

In order to improve the pressure drop characteristics, two additional cases are evaluated. These two cases are 1 mm curvilinear and four channels curvi-square with 0.55 mm in size. Fig. 18 shows comparison of all designs.

Results show that with increase in number of channels from two to four and decrease in channel size from 1 to 0.5 mm, a considerable improvement in terms of pressure drop is achieved. This comparison is made with the same total mass flow rate. With increase in number of channels, mass flow rate as well as the operating Reynolds number is decreased, resulting in a lower pressure drop. Additionally, with increased channel count and decreased size, a more uniform distribution of contact surface is apparent.

4.6. Validation of computational data

In order to validate the simulation model, fabrication and testing of flow fields based on selected materials and designs was carried out. Experiments evaluated the pressure drop across these fields with varying Reynolds number. The experimental data were collected multiple times in both an increasing and decreasing manner to ensure statistical reliability and precision of the experiment. Fig. 19 shows characteristic results for pressure drop in a straight through design simulated using the same methodology used above for the curvilinear cases. Results show close prediction of the computer simulation model. The deviation is primarily due to the

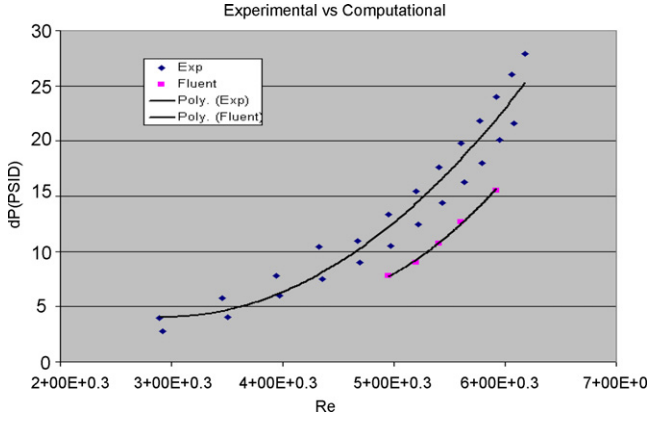

Fig. 19. Comparison of simulated pressure drop data in straight through design with experimental data.

additional losses due to the entrance and exit port of the bipolar plate where the pressure tap is located.

5. Conclusion

Bipolar plates with different shape, size and pattern of gas flow channels are analyzed using computational fluid dynamic model. Distribution of velocity and pressure are analyzed to show the effect of different serpentine channels with varying number of channel, pattern and sizes. Following conclusions can be made from the results:

- Results show developing flow pattern in the entry region of the flow channel. However, in terms of total pressure drop, a periodic fully developed pattern in achieved in three to four turns of the serpentine channel.
- Serpentine channels give rise to additional pressure losses due to the presence of flow separations and secondary flows near the inner side the bends. This is however desirable for enhanced heat and mass transfer point of view. Also, velocity and pressure drop characteristics display periodically fully developed nature by the third to fourth turns.
- The serpentine square bends exhibit consistently higher pressure drops compared to curvilinear bends.
- Use of multiple parallel serpentine channels increases contact surface area with the electrode surface, and with reduced pressure drops. Further decrease in cross-sectional area would lead to a more uniform distribution gas concentration at electrode surfaces, but with increase in pressure drop.
- The dual serpentine channels give rise to similar periodically fully developed flow in second and third turns. However, presence of flow separations and secondary flows in each bend is significantly reduced compared to single square serpentine channels.

Work now in progress to incorporate these correlations in a PEM fuel cell simulation model to evaluate the effects of bipolar plate designs on mass transfer loss, and hence on the total current and power density of the fuel cell.

Acknowledgment

The Authors are grateful for the support of this work by United States Department of Transportation under grant no.: IL-26-7006.

References

[1] A. Kumar, R.G. Reddy, J. Power Source 113 (2003) 11–18.
[2] A. Kumar, R.G. Reddy, Adv. Mater. Energy Convers. II TMS (2004) 317–324.
[3] A. Kumar, R.G. Reddy, Fundam. Adv. Mater. Energy Convers. II, TMS (2002) 41–51.
[4] D.J. Wheeler, J.S. Yi, R. Fredley, D. Yang, T. Patterson, L. VanDine, J. New Mater. Electrochem. Syst. 4 (2001) 233–238.
[5] M. Curtis, L. Xianguo, Performance modeling of a proton exchange membrane fuel cell, in: Proceedings of the 1998 ASME Energy Source Technology Conference, 1998.
[6] T. Berning, D.M. Lu, N. Djilali, J. Power Sources 106 (2002) 284–294.
[7] P.T. Nguyen, T. Berning, N. Djilali, J. Power Sources 130 (2004) 149–157.
[8] R. Boddu, P. Majumdar, Gas flow analysis of bi-polar plate designs for fuel cells, in: Proceedings of the 4th International Conference of Fuel Cell Science, Engineering and Technology, Irvine, CA, 2006, pp. 1–11, FUEL Cell2006-97122.